

Visible-Light-Responsive Photocatalysis: Ag-Doped TiO_2 Catalyst Development and Reactor Design Testing

Janelle L. Coutts[1],
Engineering Services Contract, Kennedy Space Center, FL, 32899

Paul E. Hintze[2], Anne Meier[3], Malay G. Shah[4]
NASA – Kennedy Space Center, FL, 32899

Robert W. Devor[5], Jan M. Surma[6], Phillip R. Maloney[7], Brint M. Bauer[8],
Engineering Services Contract, Kennedy Space Center, FL, 32899

and

David W. Mazyck[9]
NASA – Kennedy Space Center, FL 32899

In recent years, the alteration of titanium dioxide to become visible-light-responsive (VLR) has been a major focus in the field of photocatalysis. Currently, bare titanium dioxide requires ultraviolet light for activation due to its band gap energy of 3.2 eV. Hg-vapor fluorescent light sources are used in photocatalytic oxidation (PCO) reactors to provide adequate levels of ultraviolet light for catalyst activation; these mercury-containing lamps, however, hinder the use of this PCO technology in a spaceflight environment due to concerns over crew Hg exposure. VLR-TiO_2 would allow for use of ambient visible solar radiation or highly efficient visible wavelength LEDs, both of which would make PCO approaches more efficient, flexible, economical, and safe. Over the past three years, Kennedy Space Center has developed a VLR Ag-doped TiO_2 catalyst with a band gap of 2.72 eV and promising photocatalytic activity. Catalyst immobilization techniques, including incorporation of the catalyst into a sorbent material, were examined. Extensive modeling of a reactor test bed mimicking air duct work with throughput similar to that seen on the International Space Station was completed to determine optimal reactor design. A bench-scale reactor with the novel catalyst and high-efficiency blue LEDs was challenged with several common volatile organic compounds (VOCs) found in ISS cabin air to evaluate the system's ability to perform high-throughput trace contaminant removal. The ultimate goal for this testing was to determine if the unit would be useful in pre-heat exchanger operations to lessen condensed VOCs in recovered water thus lowering the burden of VOC removal for water purification systems.

[1] Scientist IV, ESC - Chemical & Biological Sciences, Mail Stop ESC-24, Kennedy Space Center, FL 32899.
[2] Chemist, NASA Applied Science Branch, UB-R3, Kennedy Space Center, FL 32899.
[3] Chemical Engineer, NASA Materials Analysis Branch, NE-L3, Kennedy Space Center, FL 32899.
[4] Pathways Intern, NASA-KSC, Kennedy Space Center, FL 32899.
[5] Scientist V, ESC - Chemical & Biological Sciences, Mail Stop ESC-55, Kennedy Space Center, FL 32899.
[6] Scientist IV, ESC - Chemical & Biological Sciences, Mail Stop ESC-5, Kennedy Space Center, FL 32899.
[7] Scientist IV, ESC - Chemical & Biological Sciences, Mail Stop ESC-5, Kennedy Space Center, FL 32899.
[8] Mechanical Technician, ESC - Chemical & Biological Sciences, Mail Stop ESC-55, Kennedy Space Center, FL 32899.
[9] Professor of Environmental Engineering, University of Florida, Gainesville, FL 32611.

Nomenclature

CCT = Correlated Color Temperature
CFD = Computational Fluid Dynamic
DRS = diffuse reflectance spectroscopy
eV = electron volts
GC-FID = gas chromatograph-flame ionization detector
ISS = International Space Station
KSC = Kennedy Space Center
LED = light emitting diode
MA = mechanical alloying
PCO = photocatalytic oxidation
PD = photodeposition
RANS = Raynolds-averaged Navier Stokes
STC = silica-titania composite
TCC = trace contaminant control
TEOS = tetraethyl orthosilicate
UCF = University of Central Florida
UF = University of Florida
UV = ultraviolet
VLR = visible-light-responsive
VOC = volatile organic compound
W = Watt

I. Introduction

TITANIUM dioxide has been one of the most utilized photocatalysts dominating the field of photocatalytic oxidation (PCO) for decades. Applications for this technology encompass a broad range of processes such as hydrogen production via photocatalytic water splitting, chemical and biological purification of water and air, and synthesis of organic compounds. A commercial TiO_2, Degussa P25, consisting of a mixture of anatase (70-85%), rutile, and amorphous (minor) titania[1], has demonstrated high PCO activity in numerous studies[2-7]. The anatase phase is known for its superior photocatalytic activity relative to the rutile phase[8] with a band gap energy of 3.2 eV; the Degussa P25 mixture has also demonstrated higher photocatalytic activity over pure anatase or rutile phase TiO_2[8]. Based on the anatase band gap, photons with a wavelength of 388 nm or less (i.e., UV) are required to activate anatase TiO_2[9]. Traditionally, Hg-vapor light sources are used in PCO systems, but the presence of mercury within the bulbs precludes their use in crewed spaceflight environments due to the possibility of contamination (i.e., bulb breaks). Ultraviolet LEDs are an emerging technology, and have proven to be a feasible excitation light source alternative. However, a survey of commercially-available UV-LEDs show that they possess low lighting efficiency (13%)[6].

The UV-range photonic energy requirements for bare-TiO_2 photocatalysis limits the use of traditional indoor lighting or solar radiation, which only consists of ~4-6% UV radiation at the Earth's surface[10], as conceivable energy sources. Furthermore, UV-activated photocatalysis using TiO_2 provides only a moderate reaction rate and somewhat low quantum yield due to a low electron transfer rate and high electron-hole recombination rate[11]. Thus, in its current state of development, TiO_2-assisted photocatalysis is not feasible for high throughput processes. A solution for overcoming such limitations is to enable the TiO_2 photocatalyst to be activated by visible light to allow for the use of highly efficient blue or white LEDs or visible band solar radiation (~45% of the solar spectrum lies in the visible region[10]). The development of Visible Light Responsive (VLR) PCO catalysts would facilitate the acceptance and incorporation of PCO-based technology for numerous ISS applications including use in air trace contaminant control (TCC) water recovery systems, low-cost hydrogen production using solar energy[12], enhanced chemical and microbial purification of water[13, 14], and potentially in the field of artificial photosynthesis. The past decade has witnessed a shift in catalyst development towards visible light responsiveness. Efforts have included sensitization of TiO_2 with absorbed dye molecules[15, 16], metal cation[17-21] or anion[22-24] doping, and narrow band gap semiconductor and TiO_2 coupling[25-27] to name a few. Despite the vast amount of research in this field, conclusions regarding the relative effectiveness of any given method are difficult to draw due to the lack of consistent or standardized experimental conditions.

In the past several years, a team from Kennedy Space Center (KSC) and the University of Central Florida (UCF) developed a VLR catalyst library focused on coupling narrow band gap semiconductors with TiO_2 via two methods: 1) photodeposition, and 2) mechanical alloying. Further, rapid screening assays for photocatalytic activity in both the

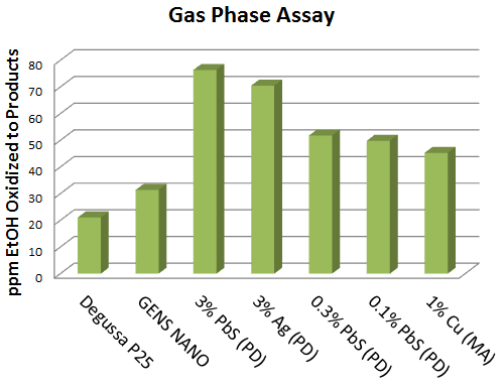

Figure 1: Gas phase ethanol oxidation to products results for top-performing catalysts compared to Degussa P25 and GENS NANO™ catalysts. PD = photodeposition method; MA = mechanical alloying method.

aqueous and gas phases were developed to allow for direct comparison of the catalysts. A total of 45 catalysts were synthesized and tested; a commercially-available VLR catalyst was also characterized[28]. Gas phase testing focused on the PCO of ethanol; the top five performing catalysts from the rapid assay are shown in Figure 1[28]. Constraints on the rapid assay reactor, a static vial, limited the analytical techniques and operational optimization available; thus, measurements focused on the oxidation of ethanol to acetaldehyde (not a favored reaction product, as acetaldehyde is more harmful than ethanol). From these results, 3%-PbS- and 3%-Ag-doped TiO_2, both prepared via the photodeposition method, were considered for future gas-phase PCO work. While the PbS-doped catalyst showed the highest relative activity, a determination was made to eliminate it as an option due to safety concerns associated with lead sulfide in air purification systems.

After the catalyst down-selection was completed from the initial rapid assay testing, the KSC team has continued work that focuses on the development of a bench-scale, high-throughput reactor incorporating the novel VLR catalyst. Catalyst immobilization techniques, including incorporation of the catalyst into a sorbent material, were examined in conjunction with the University of Florida (UF). Extensive modeling of a reactor test bed mimicking air duct work with throughput similar to that seen on the International Space Station was completed to determine optimal reactor design. High-efficiency blue LEDs were also utilized in the design to eliminate Hg-containing light sources from the system in order to better accommodate spacecraft needs. The system was challenged with several common volatile organic compounds (VOCs) found in ISS cabin air to evaluate the system's ability to perform high-throughput trace contaminant removal. The ultimate goal for this testing was to determine if the unit would be useful in pre-heat exchanger operations to lessen condensed VOCs in recovered water thus lowering the burden of VOC removal for water purification systems.

II. High-Throughput Reactor Design

A. Reactor Design Considerations

Considerations for a photocatalytic reactor concentrated on a design that could be implemented in an air duct-style system, focusing on elements allowing for high-throughput of contaminated air. A rectangular reactor design was adopted to simulate a typical air duct shape; in order to provide a low pressure drop within the system, LED and catalyst panels, parallel to the air flow, was used. By comparing dimensions, flow rates, and contact times of several commercially-available photocatalytic units tested at Marshall Space Flight Center[29], it was determined that the constructed bench scale reactor would be 6"x6"x12" long and consist of two air channels processing 25 L/min per channel. To accomplish comparable processing volumes of the commercial units (2500 L/min or 88 cfm), the bench-scale unit would need to be approximately 3.5 times larger.

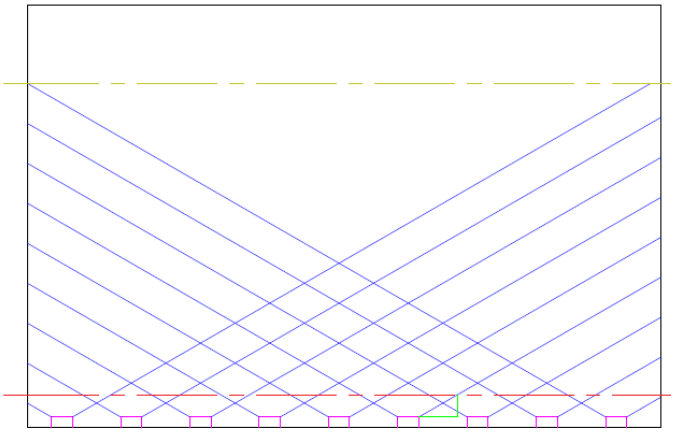

Figure 2: LED panel lighting distribution based on 120° light spread from each LED (blue); the red line indicates the minimum distance while the gold line indicates the furthest distance from the top of the LEDs to the catalyst panel.

Further analysis for determination of optimal channel height (distance between catalyst and LED panels) and catalyst panel design was also completed. The channel height is dependent on LED layout; because LEDs are a point source light, the distance between the LED panel and catalyst panel becomes a compromise between obtaining evenly distributed light and the highest possible light

intensity. Based on Figure 2, it was determined that the channel height must remain between 0.2108" and 3.1616" to achieve optimal intensity and uniform illumination.

B. Computational Fluid Dynamic (CFD) Analysis

A major consideration within the reactor design was ensuring that flow through each channel allowed for sufficient interaction of contaminants with the catalyst panel (i.e., that there was turbulent flow rather than laminar flow). In order to encourage turbulent flow, fins were attached to the catalyst panel; various configurations and sizes were explored to achieve optimal flow dynamics via Computational Fluid Dynamic (CFD) Analysis using OpenFOAM v2.4. Designs for the fin geometry iterated from discrete, alternating angled fins to continuous V-shaped fins pointing upstream. A design with parallel, angled fins was also considered but was found to perform poorly in comparison to the V-shaped fins. A successful design was chosen based on visual inspection of the results as well as the estimated pressure drop across the channel. Figure 3 shows the simulation domain for the chosen design. The channel was extended slightly at the inlet and outlet in order to avoid instabilities in the simulation.

The turbulent air flow was modeled using the SST k-omega turbulence model in a Reynolds-averaged Navier-Stokes (RANS) setup. A steady-state solver for incompressible, turbulent flows was used; this solver is called simpleFoam in OpenFOAM. It was assumed that the air can be treated as an incompressible ideal gas. No chemical reactions were modelled and any thermal effects were neglected. Boundary conditions used in the simulation included a fixed inlet velocity of 0.2691 m/s (equivalent to 25 L/min volumetric flow rate), fixed outlet pressure of 0 Pa, no-slip walls with appropriate wall functions, and a channel height of 0.4".

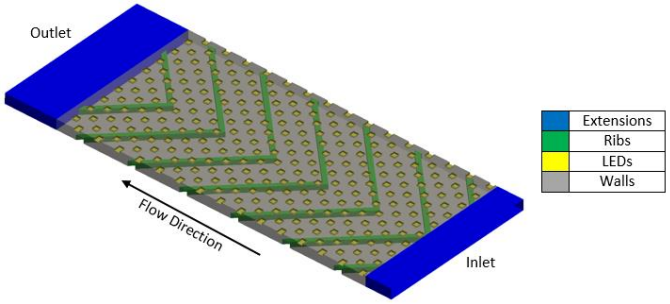

Figure 3: CFD Domain

With a flow rate of 25 L/min through a single channel, the pressure drop was fairly low: within the range of 1-2 Pa. As expected, several recirculation regions existed within the channel as air flowed through. The V-shaped fins split the flow and created two large counter-rotating vortices. Air near the bottom wall was forced outward toward the sidewalls. Along the top surface, the flow was pushed inward towards the center of the channel. Additional smaller recirculation regions formed along the immediate downstream side of the ribs. These smaller local vortices forced the air to repeatedly make contact with the surface as it travelled between fins while the large-scale rotations helped force air near the top surface downwards. The LED lights along the top surface also helped to disturb any boundary layer growth, and generally added to the turbulence within the system. The local vortices can be seen via streamlines in Figure 4. Point and line sources were used to generate streamlines through a particular set of coordinates.

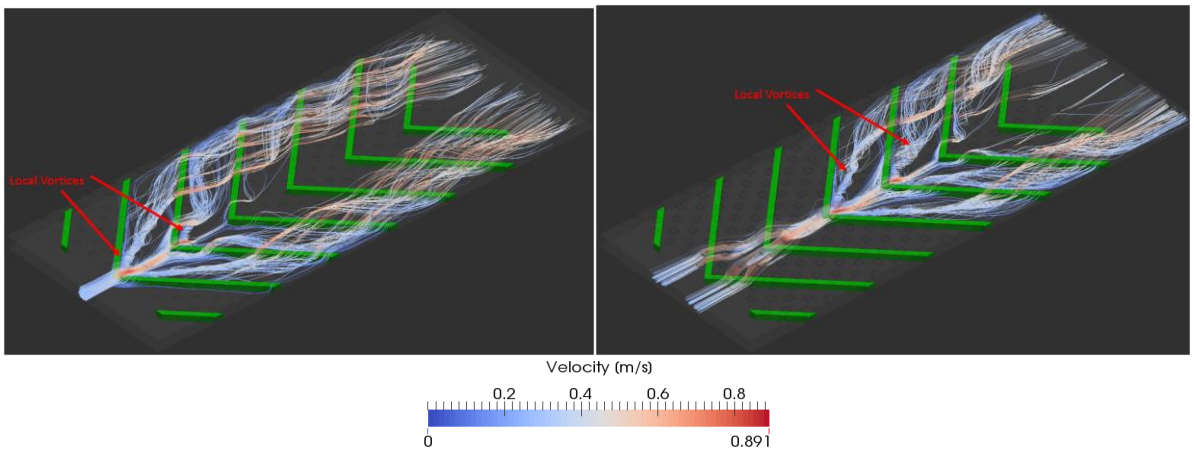

Figure 4: Point source on tip of first rib (Right); point source on tip of third rib (Left).

The large-scale rotations can be seen in Figure 5 from the line source streamlines placed at the inlet. For clarity, the streamlines were clipped to show the how the flow behaves in the top and bottom halves of the channel. In Figure 5, (A) shows streamlines from a horizontal line source along the channel center while (B) shows streamlines from a vertical line source towards the left side of the channel. Images of the top halves from both show how the flow is

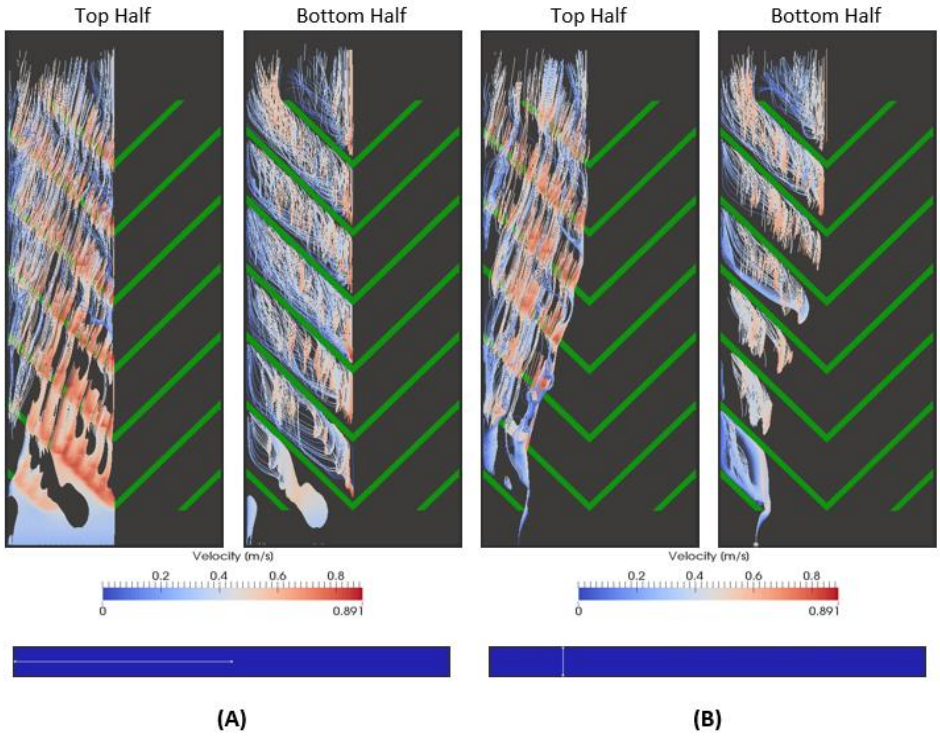

Figure 5: (A) horizontal line source; (B) vertical line source

pushed inward towards the center as it travels downstream. Along the bottom half, the flow travels outward towards the sidewall while circulating between the fins. The flow break-up as a result of the LED obstruction can also be seen near the top wall.

C. LED Light Source Selection

Two sets of LED strips were purchased for consideration in the reactor design; the first set from superbrightleds.com are described as UV/black-light LEDs with a Correlated Color Temperature (CCT) of 440 nm. According to the vendor, CCT is the measure of the color appearance of the light emitted from the light source and not necessarily the actual wavelength emitted by the source. The second set of LED strips were purchased from ledlightinghut.com and claimed to have a maximum output at 400-405nm. Irradiance profiles were collected for both brands of LED strips in a dark room using a spectroradiometer (model OL754C, Optronics Laboratories, Figure 6).

As seen in Figure 6, the superbightleds.com LEDs showed a λ_{max} of 404 nm while the ledlightinghut.com set had a λ_{max} at 406 nm, as advertised. The irradiance for a single LED was determined through the integration of the irradiation scan with defined integration limits of 5% irradiance with respect to the value at the λ_{max}; total

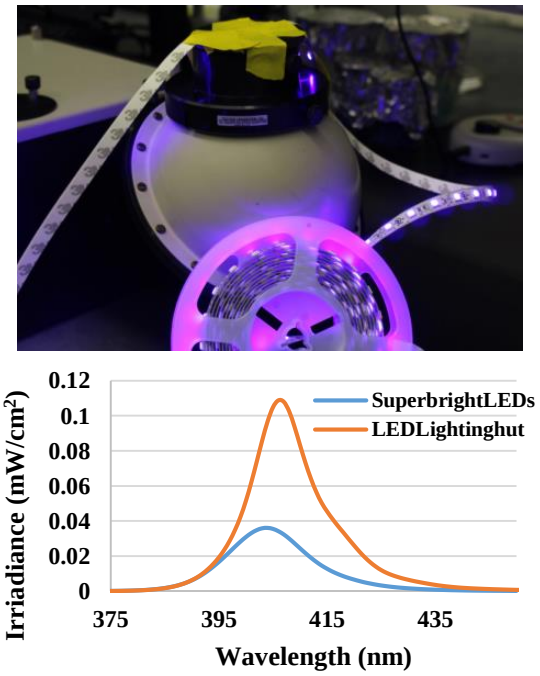

Figure 6: Spectroradiometer integrating sphere during LED profiling (Top) and irradiance profiles for LED strips (Bottom).

irradiance for this range of wavelengths was 0.692 and 1.76 mW/cm^2 for the superbrightleds.com and ledlightinghut.com LEDs, respectively. Based on these results, the ledlightinghut.com strips were selected as the light source to be used in the reactor design since they have a near 2.5x higher output than the superbrightled.com LEDs. Two 6"x12" light panels were constructed, each consisting of 234 LEDs for use within the reactor system.

III. VLR Catalyst Preparation, Immobilization, and VOC Testing Setup

D. Catalyst Preparation and Immobilization

3%-Ag-doped TiO_2 powder was prepared via photodeposition. 0.25 g of Degussa P25 titanium dioxide and 100 mL of 1:20 degassed ethanol:water were added to a 125-mL Erlenmeyer flask. An appropriate amount of 0.1 M metal to the flask to achieve a 3.0% dopant loading by weight. The flasks were placed on a stir plate approximately 3-cm from a 15W, T5 UV-A fluorescent bulb and allowed to react for 30 minutes (Figure 7). The flasks received a total of approximately 100 mW of UV radiation during the reaction. The catalyst was then centrifuged at 4500 rpm for 12 minutes to separate the solid from the liquid. The catalyst pellet was then washed and centrifuged in deionized water three times before drying at 105°C overnight.

Figure 7: Photodeposition preparation method for quantum dot formation on TiO_2.

A similar method of photodeposition was also used to dope adsorption-enhanced silica-titania-composite pellets (STCs)[4, 5, 9], containing bare Degussa P25. The STCs were 4% P25 by mass, thus requiring 556 µL of 0.1 M silver solution to 5 g of STCs to achieve the same dopant loading level. The centrifugation step described above was eliminated from the post-reaction washing steps. The pellets, shown in Figure 8, showed a thin layer of Ag-dopant on the pellet surface, indicating that the light did not penetrate completely through the pellet during photodeposition process. Traditionally, STC pellets have been used in a packed bed reactor[4, 9, 30]; with the proposed reactor design, light penetration from LED panels into a bed would not be conducive for adequate activation of the catalyst so methods to adhere the pellets to a panel were examined. An inorganic cement adhesive (Omegabond 400) was chosen over silicone- or organic-based glues to limit any possible off-gassing of VOCs which could hinder photocatalytic activity testing. It was determined that if the pellets did not have a full side adhered, they were easily brushed off the coupon. Further, creation of a tightly-packed, optimal catalyst layer proved difficult. Based on the results, the VLR catalyst powder was then incorporated into the silica composite to create a thin layer of the VLR-STC on the metal surface. The composite was prepared using tetraethyl orthosilicate (TEOS) as the silica precursor via a sol-gel technique where nitric acid and hydrofluoric acid were used to catalyze hydrolysis and condensation reactions[5]. The silica-catalyst composite was applied to 6"x12" metal plates for use in the bench-scale, high-throughput reactor via a spray coating process.

Figure 8: Small (left) and large (right) pellets after direct deposition of silver quantum dots; 3% dopant concentration was based on total weight of pellets rather than TiO_2 in pellet.

E. Catalyst Physical Characterization

1. Diffuse Reflectance Analysis

In order to determine if the emission wavelength range of the selected LEDs was suitable for the VLR catalyst activation, the band gap of the VLR catalyst was determined. A 60-mm diameter integrating sphere was mounted to a Jasco V-670 UV-visible spectrophotometer for diffuse reflectance spectra analysis of prepared bulk powder samples. A Spectralon certified reference was used as a standard. Percent reflectance was measured at ambient temperature between 300 and 800 nm at 2-nm intervals, 1000 nm/min continuous scan, with a 340-nm light source. Band-gap energy estimation was measured from the diffuse reflectance spectroscopy (DRS). Through a series of mathematical transformations[31-34], the Tauc plot is created and the tangent line at the point of inflection is drawn; the point at which the tangent line meets the x-axis equates to the band gap, Eg, value. The calculation of the band gap was completed using a Matlab script.

When photons are absorbed into a semiconductor at energy greater than the gap of the semiconductor, an electron is transferred from the valence band to the conduction band where an abrupt increase in the absorbency of the material occurs to the wavelength corresponding to the band gap energy. The relation of the absorption coefficient to the incidental photon energy depends on the type of electronic transition. When the electron momentum is conserved during the transition of electrons, the transition is direct. When the electron momentum is not conserved, and the transition requires assistance by a photon, it is it is considered an indirect transition. To analyze the electronic properties of the Ag-doped-TiO_2 samples in this experiment, the indirect transition (n=2) was used[35, 36].

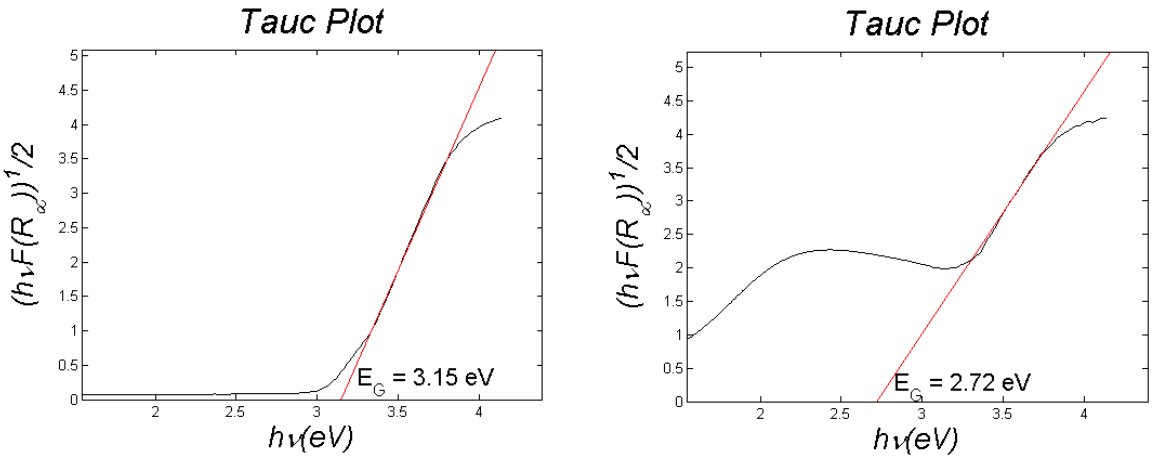

Figure 9: Tauc Plots showing band gap energies for A) Degussa P25 TiO_2 and B) 3% Ag-doped TiO_2

Figure 9 shows Tauc plots for both bare Degussa P25 TiO_2 and the VLR Ag-doped TiO_2. It is known that the band gap for anatase titanium dioxide is ~3.2 eV, and that of rutile titanium dioxide is ~3.0 eV, requiring a wavelength of 388 nm and 414 nm for activation, respectively. Degussa P25 is a mixture of anatase (70-85%) and rutile TiO_2 and has shown superior photocatalytic activity compared to either phase individually[8]. Figure 9A shows a band gap of 3.15 eV for the Degussa mixture (likely due to the high content of the anatase phase). There also exists a slight shoulder in the curve to the left of the red band gap determination line. This shoulder could be due to an impurity in the sample or partially due to the small percentage of rutile phase TiO_2 in the Degussa P25 mix. Once doped with silver, the catalyst band gap was shifted to 2.72 eV (Figure 9B); this energy correlates to activation of the catalyst by a wavelength of 457 nm or lower for activation. By using the selected LEDs with a maximum irradiance at 405 nm, activation of the dopant and the rutile phase, itself, can be accomplished for further increased photocatalytic activity. While the rutile phase is known to have inferior activity due to its direct band gap structure[8], with the presence of the anatase phase TiO_2 and VLR dopant, less electron-hole recombination events are expected due to the increased ability for charge separation and electron transfer in the material.

F. VOC Challenge Testing

1. Test Bed for VOC Challenge Testing

All experiments were performed within the developed bench-scale reactor containing two 6"x12" panels of LEDs and two 6"x12" catalyst-coated panels with V-shaped fins; each channel was 0.4" wide. CO_2-free air was supplied to a Kintek Trace Gas Generator to produce a calibrated, 2 L/min contaminant stream. This stream was then diluted with the desired flow of humidified, CO_2-free air produced by a Miller Nelson HCS-401 Flow-Temperature-Humidity Controller. All tests were carried out in a flow-through mode with a relative humidity, RH, of 30.0 ± 3.0% unless

otherwise noted) containing 25 ppm_v ethanol (Pharmco-Aaper) or 25 ppm_v toluene (Sigma Aldrich) as the test contaminant compound. Both influent and effluent streams were sampled alternately every 8.45 minutes and analyzed for the test contaminant and its oxidation intermediates by GC-FID equipped with an HP Plot Q column (30 m x 0.32 mm, 20 µm d.f.). The effluent stream was also directed to a CO_2 analyzer (Li-Cor) for the determination of the rate of CO_2 production. Data logging of parameters including relative humidity, pressure, and relative humidity, which were not recorded by the GC/FID software, was completed using a custom-programmed OPTO 22 system. Figure 10 shows the PCO test bed setup.

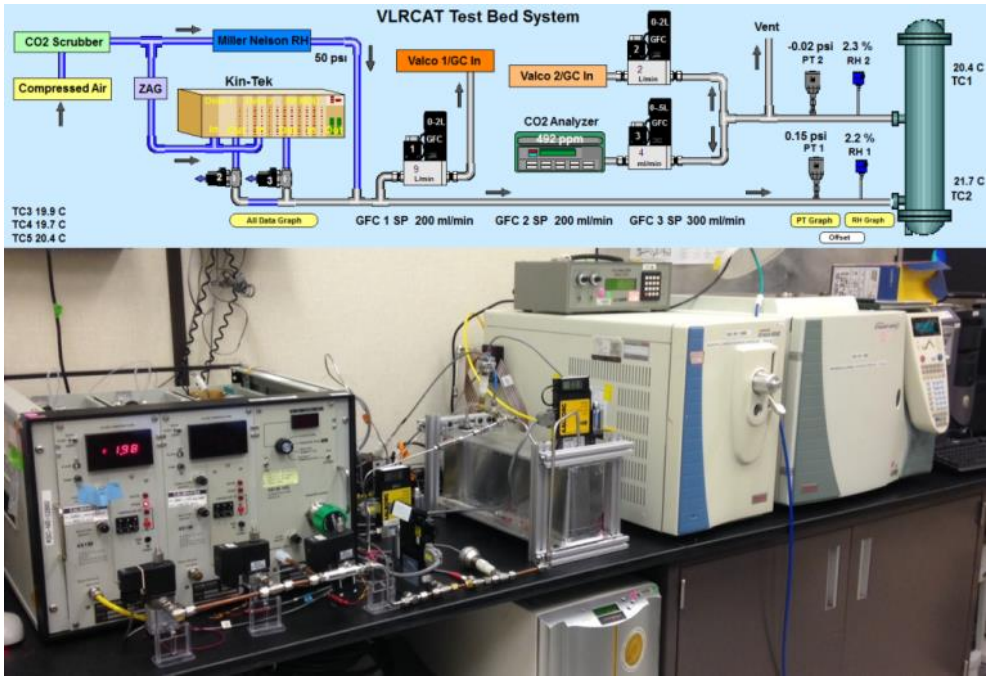

Figure 10: PCO test bed setup.

2. Calculations for PCO Oxidation Rate

PCO performance was quantified by contaminant removal: the measure of the removal of the test VOC regardless of it being adsorbed or oxidized at pseudo-steady state conditions, and mineralization efficiency (X_A), the measure of complete oxidation of the contaminant to CO_2. These values were calculated using Equations 1 and 2, respectively, where $[VOC]_{IN}$ and $[VOC]_{OUT}$ are the influent and effluent VOC concentrations; $[CO_2]_{OUT}$ is the CO_2 generated by the PCO at pseudo-steady state conditions. In Equation 2, the $[VOC]_{IN}$ is multiplied by two when ethanol is the contaminant as there are two carbons per molecule; when toluene is the contaminant, this multiplier is changed to seven. The process of mineralization typically indicates the conversion of an organic compound to an inorganic compound(s). While most definitions refer to organic compounds as any compound containing carbon, the simple oxides of carbon such as CO and CO_2 are, in this case, considered inorganic for the purpose of this definition. The rate of the PCO of the test contaminant, r, was determined based on the formation of CO_2 rather than the disappearance of the contaminant to prevent overestimation due to the VOC adsorption to the silica-rich photocatalyst. The photonic efficiency (ξ) was calculated as the ratio of the photocatalytic oxidation rate, r, to the incident photon flux, φ, as shown in Equation 3[9, 30].

$$VOC\ Removal = \left(\frac{([VOC]_{IN} - [VOC]_{OUT})}{[CO_2]_{OUT}}\right) * 100 \qquad (1)$$

$$X_A = \left(\frac{[CO_2]_{OUT}}{2*[VOC]_{IN}}\right) * 100 \qquad (2)$$

$$\xi = \frac{r}{\varphi} \qquad (3)$$

IV. Reactor Testing Results

Testing remains in progress and will be documented in the final version of the paper.

V. Conclusion

Will finish after full testing is completed.

Acknowledgments

This effort was supported by the Kennedy Space Center 2015 Center Innovation Fund (CIF).

References

1. Ohtani, B., Prieto-Mahaney, O. O., Li, D., and Abe, R. "What is Degussa (Evonik) P25? Crystalline composition analysis, reconstruction from isolated pure particles and photocatalytic activity test," *Journal of Photochemistry and Photobiology A: Chemistry* Vol. 216, No. 2–3, 2010, pp. 179-182.doi: http://dx.doi.org/10.1016/j.jphotochem.2010.07.024
2. Carp, O., Huisman, C. L., and Reller, A. "Photoinduced reactivity of titanium dioxide," *Progress in Solid State Chemistry* Vol. 32, No. 1–2, 2004, pp. 33-177.doi: http://dx.doi.org/10.1016/j.progsolidstchem.2004.08.001
3. Luo, Y., and Ollis, D. F. "Heterogeneous Photocatalytic Oxidation of Trichloroethylene and Toluene Mixtures in Air: Kinetic Promotion and Inhibition, Time-Dependent Catalyst Activity," *Journal of Catalysis* Vol. 163, No. 1, 1996, pp. 1-11.doi: http://dx.doi.org/10.1006/jcat.1996.0299
4. M. Stokke, J., Mazyck, D. W., Wu, C. Y., and Sheahan, R. "Photocatalytic oxidation of methanol using silica-titania composites in a packed-bed reactor," *Environmental Progress* Vol. 25, No. 4, 2006, pp. 312-318.doi: 10.1002/ep.10164
5. Stokke, J. M., and Mazyck, D. W. "Photocatalytic Degradation of Methanol Using Silica–Titania Composite Pellets: Effect of Pore Size on Mass Transfer and Reaction Kinetics," *Environmental Science & Technology* Vol. 42, No. 10, 2008, pp. 3808-3813.doi: 10.1021/es703221c
6. Levine, L. H., Richards, J. T., Coutts, J. L., Soler, R., Maxik, F., and Wheeler, R. M. "Feasibility of Ultraviolet-Light-Emitting Diodes as an Alternative Light Source for Photocatalysis," *Journal of the Air & Waste Management Association (Air & Waste Management Association)* Vol. 61, No. 9, 2011, pp. 932-940.doi: 10.1080/10473289.2011.596746
7. Kwon, S., Fan, M., and Cooper, A. T. "Photocatalytic Applications of Micro- and Nano-TiO2 in Environmental Engineering," *Critical Reviews in Environmental Science and Technology* Vol. 38, No. 3, 2008, pp. 197-226.doi: 10.1080/10643380701628933
8. Agrios, A. G., Gray, K. A., and Weitz, E. "Photocatalytic Transformation of 2,4,5-Trichlorophenol on TiO2 under Sub-Band-Gap Illumination," *Langmuir* Vol. 19, No. 4, 2003, pp. 1402-1409.doi: 10.1021/la026397x
9. Coutts, J. L., Levine, L. H., Richards, J. T., and Mazyck, D. W. "The effect of photon source on heterogeneous photocatalytic oxidation of ethanol by a silica–titania composite," *Journal of Photochemistry and Photobiology A: Chemistry* Vol. 225, No. 1, 2011, pp. 58-64.doi: http://dx.doi.org/10.1016/j.jphotochem.2011.09.026
10. Zayat, M., Garcia-Parejo, P., and Levy, D. "Preventing UV-light damage of light sensitive materials using a highly protective UV-absorbing coating," *Chemical Society Reviews* Vol. 36, No. 8, 2007, pp. 1270-1281.
11. Lanfang, L., Janelle, C., Jeffrey, R., Paul, H., and Christian, C. "Review on Transforming TiO2 into a Visible-Light-Responsive Catalyst for Water and Air Purification," *42nd International Conference on Environmental Systems*. American Institute of Aeronautics and Astronautics, 2012.
12. Maeda, K., and Domen, K. "Photocatalytic water splitting: recent progress and future challenges," *The Journal of Physical Chemistry Letters* Vol. 1, No. 18, 2010, pp. 2655-2661.
13. Byrne, J. A., Fernandez-Ibañez, P. A., Dunlop, P. S., Alrousan, D., and Hamilton, J. W. "Photocatalytic enhancement for solar disinfection of water: a review," *International Journal of Photoenergy* Vol. 2011, 2011.
14. Malato, S., Fernández-Ibáñez, P., Maldonado, M., Blanco, J., and Gernjak, W. "Decontamination and disinfection of water by solar photocatalysis: recent overview and trends," *Catalysis Today* Vol. 147, No. 1, 2009, pp. 1-59.
15. Grätzel, M. "Photoelectrochemical cells," *Nature* Vol. 414, No. 6861, 2001, pp. 338-344.
16. Snaith, H. J., and Schmidt-Mende, L. "Advances in liquid-electrolyte and solid-state dye-sensitized solar cells," *Advanced Materials* Vol. 19, No. 20, 2007, pp. 3187-3200.
17. Anpo, M. "Use of visible light. Second-generation titanium oxide photocatalysts prepared by the application of an advanced metal ion-implantation method," *Pure and applied chemistry* Vol. 72, No. 9, 2000, pp. 1787-1792.
18. Anpo, M., Ichihashi, Y., Takeuchi, M., and Yamashita, H. "Design of unique titanium oxide photocatalysts by an advanced metal ion-implantation method and photocatalytic reactions under visible light irradiation," *Research on chemical intermediates* Vol. 24, No. 2, 1998, pp. 143-149.
19. Asahi, R., Morikawa, T., Ohwaki, T., Aoki, K., and Taga, Y. "Visible-light photocatalysis in nitrogen-doped titanium oxides," *science* Vol. 293, No. 5528, 2001, pp. 269-271.
20. Choi, W., Termin, A., and Hoffmann, M. R. "The role of metal ion dopants in quantum-sized TiO2: correlation between photoreactivity and charge carrier recombination dynamics," *The Journal of Physical Chemistry* Vol. 98, No. 51, 1994, pp. 13669-13679.

21. Li, X., Li, F., Yang, C., and Ge, W. "Photocatalytic activity of WO x-TiO 2 under visible light irradiation," *Journal of Photochemistry and Photobiology A: Chemistry* Vol. 141, No. 2, 2001, pp. 209-217.
22. Ohno, T., Akiyoshi, M., Umebayashi, T., Asai, K., Mitsui, T., and Matsumura, M. "Preparation of S-doped TiO 2 photocatalysts and their photocatalytic activities under visible light," *Applied Catalysis A: General* Vol. 265, No. 1, 2004, pp. 115-121.
23. Rengifo-Herrera, J., Kiwi, J., and Pulgarin, C. "N, S co-doped and N-doped Degussa P-25 powders with visible light response prepared by mechanical mixing of thiourea and urea. Reactivity towards E. coli inactivation and phenol oxidation," *Journal of Photochemistry and Photobiology A: Chemistry* Vol. 205, No. 2, 2009, pp. 109-115.
24. Rengifo-Herrera, J. A., Pierzchała, K., Sienkiewicz, A., Forró, L., Kiwi, J., Moser, J. E., and Pulgarin, C. "Synthesis, characterization, and photocatalytic activities of nanoparticulate N, S-codoped TiO2 having different surface-to-volume ratios," *The Journal of Physical Chemistry C* Vol. 114, No. 6, 2010, pp. 2717-2723.
25. Gao, B., Kim, Y. J., Chakraborty, A. K., and Lee, W. I. "Efficient decomposition of organic compounds with FeTiO 3/TiO 2 heterojunction under visible light irradiation," *Applied Catalysis B: Environmental* Vol. 83, No. 3, 2008, pp. 202-207.
26. Kim, Y. J., Gao, B., Han, S. Y., Jung, M. H., Chakraborty, A. K., Ko, T., Lee, C., and Lee, W. I. "Heterojunction of FeTiO3 nanodisc and TiO2 nanoparticle for a novel visible light photocatalyst," *The Journal of Physical Chemistry C* Vol. 113, No. 44, 2009, pp. 19179-19184.
27. Kang, M. G., Han, H.-E., and Kim, K.-J. "Enhanced photodecomposition of 4-chlorophenol in aqueous solution by deposition of CdS on TiO 2," *Journal of Photochemistry and Photobiology A: Chemistry* Vol. 125, No. 1, 1999, pp. 119-125.
28. Coutts, J. L. H., Paul E.; Clausen, Christian A.; Richards, Jeffrey, T. "Visible-Light-Responsive Catalysts Using Quantum Dot-Modified TiO2 for Air and Water Purification," *44th International Conference on Environmental Systems*, Tucson, AZ, July 2014.
29. Jay, P., Kenneth, F., Joseph, S., and Dana, R. "A Comparison of Photocatalytic Oxidation Reactor Performance for Spacecraft Cabin Trace Contaminant Control Applications," *41st International Conference on Environmental Systems*. American Institute of Aeronautics and Astronautics, 2011.
30. Coutts, J. L. "TRACE CONTAMINANT CONTROL: AN IN-DEPTH STUDY OF A SILICA-TITANIA COMPOSITE FOR PHOTOCATALYTIC REMEDIATION OF CLOSED-ENIVRONMENT HABITAT AIR." University of Central Florida Orlando, Florida, 2013.
31. Murphy, A. "Band-gap determination from diffuse reflectance measurements of semiconductor films, and application to photoelectrochemical water-splitting," *Solar Energy Materials and Solar Cells* Vol. 91, No. 14, 2007, pp. 1326-1337.
32. Tauc, J., Grigorovici, R., and Vancu, A. "Optical properties and electronic structure of amorphous germanium," *physica status solidi (b)* Vol. 15, No. 2, 1966, pp. 627-637.
33. Tauc, J., and Abeles, F. *Optical properties of solids*: North-Holland, Amsterdam, 1972.
34. Davis, E., and Mott, N. "Conduction in non-crystalline systems V. Conductivity, optical absorption and photoconductivity in amorphous semiconductors," *Philosophical Magazine* Vol. 22, No. 179, 1970, pp. 0903-0922.
35. Willardson, R. K., and Beer, A. C. *Optical properties of III-V compounds*: Academic Press, 1967.
36. Dressel, M. "Gruner; G. Electrodynamics of Solids: Optical Properties of Electrons in Matter." Cambridge University Press: Cambridge, 2002.